Research Article

iMedPub Journals
www.imedpub.com

Insights in Pediatric Cardiology

2018
Vol. 2 No. 1:3

Computational Fluid Dynamics Characterization of Pulsatile Flow in a Bidirectional Glenn Shunt Supplemented with a Modified Blalock-Taussig Shunt: Flow Vortices Augment Pulmonary Artery Wall Shear Stress and Worsen Power Loss

Seda Aslan[1], Martin Guillot[1], Nancy Ross Ascuitto[2] and Robert Ascuitto[2*]

1 Department of Mechanical Engineering, University of New Orleans, LA, USA
2 Pediatric and Adult Congenital Cardiology (LLC), 27 Killdeer Street, New Orleans, LA, USA

***Corresponding author:** Ross-Ascuitto N

nrossascuitto@yahoo.com

Pediatric and Adult Congenital Cardiology (LLC), 27 Killdeer Street, New Orleans,LA-70124, USA.

Citation: Aslan S, Guillot M, AscuittoNR Ascuitto R (2018) Computational Fluid Dynamics Characterization of Pulsatile Flow in a Bidirectional Glenn Shunt Supplemented with a Modified Blalock-Taussig Shunt: Flow Vortices Augment Pulmonary Artery Wall Shear Stress and Worsen Power Loss. Insights Pediatr Cardiol Vol. 2 No.1:3.

Abstract

Background: The bidirectional Glenn shunt (BGS'S), superior vena cava (SVC) to right pulmonary artery (RPA), has become an important step in the surgical management of infants and children with single-ventricle heart disease. In some patients, however, the BGS'S is inadequate to maintain satisfactory pulmonary artery (PA) growth, in part due to a lack of pulsatile flow. In these cases, the BGS'S is often supplemented with a modified Blalock-Taussig shunt (mBTS) connected to the left pulmonary artery (LPA). Little is known about the hemodynamic consequences of combining BGS'S (low velocity passive) with mBTS (high velocity pulsatile) flow. Thus, the objective of this study is to employ simulations of cavopulmonary pathways, based on angiography, and computational fluid dynamics (CFD), using in vivo flow rates and pressures, to determine blood flow characteristics in a BGS'S supplemented with a mBTS. We focused on the flow-vessel wall interaction through wall shear stress (WSS), which plays a fundamental role in PA growth, thrombus formation and power loss, critical factors involved in the management of patients awaiting Fontan completion.

Methods: We employed a CFD model of pulsatile fluid flow, using the finite volume method, in conjunction with a non-Newtonian description of viscosity, to gain insight into blood flow behavior in a BGS'S combined with a mBTS. Our approach allows quantitative assessment of pressure distribution, flow-velocity field, WSS profile and regional power loss. The computational domain included simulations of the internal jugular, subclavian and innominate veins, SVC, central RPA and LPA with first- order branches and the mBTS. Clinically relevant boundary conditions were employed in solving the Navier-Stokes equations describing the fluid's motion. These conditions included reported sizes and flow rates of systemic veins leading to the SVC, measured pressure in the ascending aorta for the inlet to the mBTS and recorded pressures in outlets of central PA first-order branches. The hemodynamic consequences of connecting a mBTS to the PAs, or directly to the SVC, were considered.

Findings: For a planar reproduction of a BGS'S supplemented with a 4 mm mBTS connected to the LPA, the pressure in the SVC became 16.4 mmHg (peak systole), 10.2 mmHg (end diastole) and 14.5 mmHg (averaged over the cardiac cycle), consistent with the representative pressure of 12 mmHg (averaged over the cardiac cycle) at the outlets of the central PA first- order branches. The mBTS's high velocity (3-4 L/min) jet interacting with BGS'S low-velocity (0.2-0.3 L/min) flow created counter- rotating, power- depleting vortices in the cross-sectional plane of the LPA. These vortices markedly increased WSS in the LPA to 53.7 Pa (averaged over the luminal area, and the cardiac cycle), compared to ~ 0.9 Pa for

the PAs with a BGS'S alone, and ~ 2 Pa in the PAs of a normal heart. Such a high WSS in the PAs can produces intimal dysfunction, which can: enhance endothelial cell expression of coagulatory molecules and initiate platelet aggregation. However, as flow advanced from the LPA to the RPA, WSS was found to dramatically decrease to 6.2 Pa as power dissipation increased, indicative of decelerating flow. This feature of the shear stress field is critically important, as recent in vitro studies have demonstrated that high WSS's harmful effects on endothelial function are lessened when the imposed WSS possesses a negative spatial gradient, i.e, is associated with decelerating flow. The overall power efficiency (PE) for the BGS'S with a 4 mm mBTS was only ~30%, compared to 96% for the BGS'S alone. Similar results were obtained when the mBTS was attached at the origin of the branch PAs. In contrast, connecting the mBTS directly to the SVC resulted in a lower WSS burden and less flow-energy loss in the PAs.

Conclusions: BGS'S hemodynamics is greatly influenced by the addition of a mBTS. The SVC pressure becomes pulsatile and moderately increases and flow is disrupted, as anticipated. Counter- rotating vortices are established in the PAs juxtaposed to the insertion of the mBTS. These vortices can augment WSS to levels conducive to endothelial cell dysfunction, thrombus formation and worsening power loss, which are well-recognized complications with single- ventricle palliation. Nevertheless, the WSS distribution in the PAs was found to possess a spatial characteristic that has been shown to lessen flow fields' adverse shearing effects on vessels' luminal wall.

Keywords: Bidirectional-Glenn, Blalock-Taussig, Shunts, Fluid dynamics

Received: October 10, 2017; **Accepted:** March 05, 2018; **Published:** May 09, 2018

Introduction

The bidirectional Glenn shunt (BGS'S) has become a cornerstone in the staged surgical management of patients with single-ventricle heart disease. It involves detaching the superior vena cava (SVC) from the right atrium and anastomosing it directly to the nearby right pulmonary artery (RPA) [1]. It is generally performed at ~ 4 months of age. In general, the BGS'S has provided good palliation, while awaiting Fontan completion [2-3]. However, in some patients, because the SVC is the only source of blood flow to the lungs, the BGS'S has been insufficient to maintain adequate systemic arterial hemoglobin oxygen saturation and/or PA growth [4]. Under these circumstances, the final stage of the Fontan procedure is usually delayed, and the existing BGS'S is instead provided with an additional source of pulmonary blood flow, often from a modified Blalock-Taussig shunt (mBTS) connected to the LPA [5].

Proponents of this approach suggest this modification is beneficial, as it improves systemic arterial oxygen levels and provides pulsatile flow to the PAs, which is an important stimulus for their growth [6-7]. The presence of a mBTS also decreases the likelihood of developing intrapulmonary arteriovenous malformations. Conversely, opponents have raised concerns about adding a mBTS, since it sustains a volume load on the single ventricle and elevates systemic venous pressure [7]. As a consequence of these divergent views, employing a BGS'S in conjunction with a mBTS remains controversial, and its use is often based on the surgeon's preference or institutional practice. However, information is limited detailing how a mBTS influences blood flow behavior in Glenn geometries [8-11]. Thus, a quantitative evaluation of the hemodynamics associated with a BGS'S supplemented with a mBTS warrants further investigation. It is hoped insight gleaned from this type of study will help in deciding whether or not this additional surgical procedure can better prepare the PAs, in selected patients, for Fontan completion.

Blood flowing in the PAs (or any vessel), by virtue of viscosity, imparts a dissipative force along the luminal wall (per unit area), known as hemodynamic WSS. The magnitude of the WSS in straight vessels has been estimated as being directly proportional to the viscosity of the blood and flow rate, and inversely proportional to the third power of the inner radius. As a monolayer of cells in direct contact with blood flow, the endothelial lining of vessels is highly sensitive to the imposed WSS. Physiological changes in WSS help maintain vascular tone; whereas, abnormal WSSs (high and/or low) can alter endothelial cell structure, which over time can lead to destructive remodeling of the vessel wall [12]. Moreover, under certain blood flow conditions, resultant high WSS has been implicated in the development of endothelial phenotypic changes and a transcriptional profile resulting in site-specific susceptibility to thrombus formation [13,14] and/or fibrointimal hyperplasia [15]. Thus, our computational simulation study is designed to assess the nature of the blood flow- WSS nexus, and

how this interaction may affect endothelial function. We focused on WSS, as it is the primary determinant of PA growth and power loss, both of which can impair lung perfusion [16].

We employed reproductions of the cavopulmonary pathway, based on angiography, and computational fluid dynamics (CFD), using measured *in vivo* flows and pressures, to determine pulsatile flow characteristics in a BGS'S supplemented with a mBTS. Since flow shear rates are relatively low in the systemic venous system, but can vary considerably under pulsatile conditions, we incorporated a non-Newtonian model of blood viscosity, see Appendix A. In doing so, we focused on the central PAs, and determined: pressure distribution, flow-velocity field, WSS profile and power loss. We hypothesized that, addition of a mBTS would: "1) create elevated cyclic pressure and disrupt flow in the SVC and 2), in analogy to fluid traversing a bend in a vessel, give rise to counter- rotating vortices in the cross-sectional plane of the PAs, which can increase local WSS and thereby worsen power dissipation, as a consequence of the mBTS's (high-velocity) jet mixing with the BGS'S's (low-velocity) flow".

CFD simulations enabled us to characterize the flow field, determine the resultant WSS distribution and quantify regional power loss in the cavopulmonary pathway, which cannot be obtained directly, *in vivo*. Furthermore, we gained insight into: 1) how flow behavior can give rise to abnormally high and/or low WSS and 2) that WSS with a negative spatial gradient (decelerating flow) may be less deleterious to endothelial cell function. Such information can potentially lead to improved strategies in the management of certain single ventricle patients awaiting Fontan completion.

Methods

Model Parameters:

Fluid is assumed to be incompressible, with a density (ρ) of 1060 kg/m^3. Shunt and vessel walls are assumed to be rigid and impermeable. Fluid pressure is expressed in Pascal-Pa (N/m^2), or mmHg, depending on the information being presented. One Pa = 1N/m^2 and 1mm Hg = 133.32 Pa. Volumetric flow rate is expressed in L/min, and 1L/min = 1.66 x 10^{-5} m^3/s. Flow-velocity is expressed in m/s.

Reproductions of a Bidirectional Glenn Shunt (BGS'S) Supplemented with a Left Modified Blalock-Taussig Shunt (mBTS):

In the first part (I) of this study, we employed a planar reproduction of the general shape of a BGS'S supplemented with a left mBTS, based on angiograms for a typical clinical case of a 3-4 year old with stage 2 palliation for single ventricle (Figure 1). In this model, we used an expanded anatomical domain in order to account for the major systemic veins providing blood flow to the SVC; namely, the right internal jugular vein (R- IJV) and right subclavian vein (R- SCV), the L- IJV and L- SCV, the right innominate vein (R- INV) and L- INV. The domain also included the segment of the SVC comprising the BGS'S and the central RPA and LPA, respectively, along with first-order branches. The vessels and shunts were taken to be tubular with circular cross-sectional areas. Their axes were assumed to lie in a "single" plane (X,Y), chosen as the fluid dynamics anterior/posterior symmetry plane.

For this model, vessel sizes were obtained from reported values for children and young adults. The R- INV, L- INV and SVC diameters (and lengths) have been shown to correlate closely with patient height [17]. For a height of 100 cm, typical for a 3-4 year old, and using linear regression analysis, representative values are: R- INV 9.8 mm (10 mm), L- INV 9.8 mm (32 mm) and SVC 12.5 mm (39 mm). The R- IJV, R- SCV, L- IJV and L- SCV diameters (and lengths) were determined from ultra-sonographic studies in children [18-20], and by scaling from corresponding vessel sizes in young adults. Representative values are: R- IJV 6.9 mm (20 mm), R- SCV 4.9 mm (20 mm), L- IJV 6.9 mm (20 mm) and L- SCV 4.9 mm (20 mm). The central RPA and LPA diameters (and lengths) have been shown to correlate well with patient BSA [21]. For a BSA of 0.65 m^2 and Z-score of 0, representative values are: RPA 9.0 mm (24.5 mm) and LPA 9.0 mm (24.5 mm), with upper and lower branches of 4.5 mm and 7.0 mm, respectively. The mBTSs considered were 4 mm (40 mm) and 5 mm (40 mm). The distance between the mid-line of the SVC and the central axis of the mBTS is 28 mm (Table 1).

Inlet and Outlet Boundary Conditions:

For all calculations, we assumed flow- velocity to be zero at the inner vessel (or shunt) wall. The R- IJV, R- SCV, L- IJV and L- SCV flow rates were determined from Doppler flow-velocity studies in children [22,23], and by scaling from flow rates for young adults [24]. Our desire was to impose inlet boundary conditions for vessels at sites proximal to the anatomical region of interest. The flow rates in the systemic veins were held fixed and representative values are: R-IJV 0.28 L/min, R-SCV 0.19 L/min, L-IJV 0.31 L/min and L- SCV 0.22 L/min. At the entrance to the R-IJV, R- SCV, L-IJV and L-SCV, flow was well developed and the velocity profiles were essentially parabolic. The corresponding flow rates in the R-INV and L-INV are 0.47 L/min and 0.53 L/min, respectively. Thus, net flow rate entering the SVC from the systemic veins was 1 L/min (Table 1).

Cardiac catheterization data, for our prototypic patient, were used to specify representative pressures employed for boundary conditions. At the inlet to the mBTS, the representative pressure, as a function of time, was taken as the recorded pressure in the ascending aorta over the cardiac cycle (Figure 2a). For such a pressure boundary condition, the computational program assumes a spatially- uniform velocity profile at the inlet to the shunt, which is computed as part of the overall solution. At the outlets of the central PA first- order branches, the recorded pressures, as a function of time, were found to be very similar. Thus, for each of the branches, the representative pressure was taken to be that in (Figure 2b). Simulated first-order branches were included in the computational model primarily to yield more realistic velocity distributions for the outgoing flows, and the representative pressure at the outlets was used to provide a component of afterload for the simulated cavopulmonay pathway.

In the second part (II) of this study, we accounted for the LPA generally being posteriorly and inferiorly oriented with respect to

the RPA, (Figure 3). The axis of the LPA was rotated ~ 45° posterior and ~ 25° inferior to that of the RPA, as guided by angiography. The boundary conditions at the inlets and outlets of the fluid pathway were taken to be the same as those used in the first part (I) of this study.

In the third part (III) of this study, we returned to the planar representation in (Figure 1). First, the 4 mm mBTS was envisioned as attached directly to the SVC, mid-way along its medial side, at an angle of ~ 45°. The ratio of the diameter of the mBTS to that of the SVC is 0.32. Second, the 4 mm mBTS was considered to be connected to the SVC, between the R- INV and L- INV. For both these arrangements, the boundary conditions at the inlets and outlets of the fluid pathway were taken to be the same as those used in the first part (I) and the second part (II) of this study.

Computational Fluid Dynamics (CFD):

"Flow studies were conducted using the commercial CFD software package Fluent 15 (Ansys, Inc., Lebanon, NH, USA). Fluent is a general purpose computer program capable of numerically solving the 3-dimensional (3-D) Navier- Stokes and continuity equations using the finite volume method, once the boundary conditions are defined [25].

The Navier- Stokes equations may be written as follows:

$$\rho(\partial \vec{V} / \partial t + \vec{V} . \vec{\vec{T}}) = -\nabla p + \eta a \vec{\nabla} . \vec{\vec{T}} \quad (1)$$

Where

$$\vec{\vec{T}} = \vec{\nabla} \vec{V} \quad (2)$$

The quantity T is a shear stress tensor, and ηa is the apparent viscosity. Here V denotes the fluid velocity vector, with components Vx, Vy and Vz, in the x, y, and z directions, respectively, and (p) is the local static pressure (henceforth referred to simply as pressure).

The corresponding continuity equation is:

$$\vec{\nabla} . \vec{V} = 0 \quad (3)$$

Finite Volume Method:

Fluent uses the finite volume method to discretize the N-S equations, where the fluid domain is divided into a number of volumetric elements called cells. The equations are integrated within each cell, and convective and diffusive fluxes are interfaced across cells. We used a fully-coupled method for all computations with 2nd order up-winding for the convective terms. We used tetrahedral cells throughout, along with prismatic cells near vessel walls. Typically, 1,500,000 cells are required, with 9 layers of prismatic cells near the walls, to accurately capture the velocity gradients required to compute WSSs.

Wall Shear Stress:

Based on equation 2, the magnitude of the local WSS (τ_w) is directly proportional to the product of η_a and the shear rate $\tau_w = \eta_a (\Delta V_{t/} \Delta r)$ at the vessel wall;

Here, V_t is the fluid's local velocity component tangent (parallel) to the wall and (r) is a distance normal to the wall. Thus, γ represents the change in tangential velocity per unit distance. For uniform flow in a straight vessel of radius R, ($\Delta V_{t/} \Delta r$) is ~ <Q>/R^3, where <Q> is the average flow. However, for a non-Newtonian fluid, η_a depends on γ. In the limit of high γ, η_a approaches a constant value, which was taken as 3.45 x 10^{-3} kg/m-s; it corresponds to hematocrits of 33 - 45%. The Carreau model of blood was chosen to describe η_a's dependence on γ, see Appendix A [26]. Wall shear stress is expressed in units of (Pa).

Power Efficiency for a Fluid Flow Transition:

The power efficiency (PE) for the overall fluid transition, i.e. from the inlets (i) to the outlets (f) of the cavopulmonary pathway, over the cardiac cycle (T), is taken as:

$$PE_{i,f} = 1/T \int [1 - \{\Delta W_{i,f}(t) / W_i(t)\}] \, dt \times 100\% \quad (4)$$

The quantity $^{\Delta W}_{i,f}$ (t) represents the instantaneous power loss (i to f), i.e. the flow's mechanical energy dissipated per time, and W_i (t) is the flow's incoming power at time (t). The powers are expressed in Watts (W) or Joules (J)/s (Appendix B).

Results

BGS'S in the Absence of a Left mBTS

The pressure in the SVC averaged 1638 N/m² or 12.3 mmHg, consistent with the assumed pressure of 1600 N/m² or 12 mmHg, at the outlets of the central PA first-order branches (Table 2). (Figure 4) shows the magnitude of the flow velocity, as projected onto the longitudinal (mid-axial) plane of the cavopulmonary pathway. Streaming of flow in the SVC (red regions) was present, and primarily determined by the relative orientation of the INVs. The flow velocity in the SVC and in the central PAs was low, typically ~ 0.13 m/s. Figure 5 shows a contour plot of the magnitude of the WSS. The WSS (averaged over the luminal area) for the SVC was 0.7 Pa, for the central RPA and LPA was 1.2 Pa and 0.7 Pa, respectively, and for the central (RPA plus LPA) was 0.9 Pa. At vascular connections, e.g. IJVs to the INVs and SVC to the RPA, where flow underwent abrupt change in direction, WSS typically increased to ~ 2.0 Pa (red regions); at one site it reached ~ 3.8 Pa. The power loss (ΔW) in the SVC was 0.18 mW, and in the central (RPA plus LPA) totaled 0.20 mW. The overall PE for the system was 96%.

Part I (A): BGS'S Supplemented with a 4 mm Left mBTS (Figure 1):

The pressure in the SVC averaged 2191 N/m² or 16.4 mmHg (at peak systole) and 1367 N/m² or 10.2 mmHg (at end diastole). It was 1910 N/m² or 14.3 mmHg (averaged over the cardiac cycle), consistent with the representative pressure of 1600 N/m² or 12 mmHg (averaged over the cardiac cycle), at the outlets of the central PA first-order branches (Table 2, Figure 6) shows the magnitude of the flow velocity, as projected onto the longitudinal (mid-axial) plane of the cavopulmonary pathway (at peak systole). Streaming of flow in the INVs and SVC (light blue regions) was still evident. The flow velocity in the SVC was low at ~ 0.25 m/s (dark blue region) and in the central PAs it increased to ~ 0.6 m/s (light blue region). Conversely, velocity in the mBTS was high at 3-4 m/s (red region).

Figure 7a shows the magnitude of the velocity, as projected onto the cross-sectional plane, at the axis of the mBTS (at peak systole). The mBTS's jet (red region) penetrated into the LPA and, in doing so, reached the inferior wall, where a stagnation point (small blue area) was created. At this site, the jet initiated secondary flow along the anterior and posterior side walls (narrow red regions) of the LPA, to form counter-rotating vortices (large curved black arrows). Figure 7b shows the magnitude of the velocity, as projected onto the cross-sectional plane, now at the axis of the SVC (at peak systole). The slowly-moving flow in the SVC (large slightly- curved black arrows) upon entering the RPA encountered flow advancing from the left mBTS. Their interaction led to an interconnection of the vortices (large curved black arrows), which penetrated into the SVC.

(Figure 8) shows a contour plot of the magnitude of the WSS (at peak systole). The counter- rotating vortices markedly increased local WSS to 280 Pa (red annular region surrounding a stagnation point of low WSS- denoted in blue), on the inferior luminal surface of the LPA (see insert). A similar pattern persisted with WSS decreasing to 168 Pa (at end diastole- not shown). The WSS (averaged over the luminal area, and the cardiac cycle) for the SVC was 0.8 Pa, for the mBTS was 28.4 Pa, for the central RPA and LPA was 6.2 Pa and 53.7 Pa, respectively, and for the central (RPA plus LPA) was 30.4 Pa. The power loss ΔW (averaged over the cardiac cycle) in the SVC was 0.27 mW, in the mBTS was 0.05 W and in the central (RPA plus LPA) totaled 0.14 W. Thus, dissipative power loss was greatest in the PAs. The overall PE for the system was 31%.

Part I (B): BGS'S Supplemented with a Repositioned 4 mm Left mBTS

In this case, the 4 mm mBTS was inserted at the origin of the central RPA and LPA, i.e. along the dashed vertical line in Figure 1. The pressure in the SVC averaged 2252 N/m^2 or 16.9 mmHg (at peak systole) and 1334 N/m^2 or 10.0 mmHg (at end diastole). It was 1869 N/m^2 or 14.0 mmHg (averaged over the cardiac cycle). Incoming flow from the mBTS increased local WSS to 277 Pa (at peak systole) on the inferior luminal surface of the PAs, across from the insertion of the mBTS. The WSS (averaged over the luminal area, and the cardiac cycle) for the central RPA and LPA was 31.6 Pa and 31.4 Pa, respectively, and for the central (RPA plus LPA) was 31.5 Pa. The ΔW (averaged over the cardiac cycle) in the central (RPA plus LPA) totaled 0.14 W. The overall PE for the system was 31 %.

Part I (C): BGS'S Supplemented with a 5 mm Left mBTS

In this case, the 4 mBTS in Figure 1 was replaced with a 5 mm mBTS. The pressure in the SVC averaged 2338 N/m^2 or 17.5 mmHg (at peak systole) and 1518 N/m^2 or 11.4 mmHg (at end diastole). It was 2062 N/m^2 or 15.5 mmHg (averaged over the cardiac cycle). Incoming flow from the mBTS increased local WSS to 283 Pa (at peak systole), on the inferior luminal surface of the LPA (recall Figure 8-see insert). The WSS (averaged over the luminal area, and the cardiac cycle) for the central RPA and LPA was 11.7 Pa and 64.4 Pa, respectively, and for the central (RPA plus LPA) was 39.4 Pa. The ΔW (averaged over the cardiac cycle) in the central (RPA plus LPA) totaled 0.21 W (~ 50% greater than for the 4 mm mBTS in Figure 1). The overall PE for the system was 29%.

Part II (A): BGS'S Supplemented with a 4 mm left mBTS, and an Angulated LPA (Figure 3):

In this case, the LPA was angled with respect to the RPA. The pressure in the SVC averaged 2161 N/m^2 or 16.2 mmHg (at peak systole) and 1377 N/m^2 or 10.3 mmHg (at end diastole). It was 1854 N/m^2 or 13.9 mmHg (averaged over the cardiac cycle). Incoming flow from mBTS increased local WSS to 289 Pa (at peak systole), on the inferior luminal surface of the LPA. The WSS (averaged over the luminal area, and the cardiac cycle) for the central RPA and LPA was 6.9 Pa and 51.2 Pa, respectively, and for the central (RPA plus LPA) was 29.3 Pa. The ΔW (averaged over the cardiac cycle) in the central (RPA plus LPA) totaled 0.11 W (slightly lower than for the non-angulated LPA). The overall PE for the system was 33%.

Part II (B): BGS'S Supplemented with a Repositioned 4 mm left mBTS, and an Angulated LPA:

In this case, the LPA was again angled with respect to the RPA. The 4 mm mBTS was inserted at the origin of the central RPA and LPA, i.e. along the dashed vertical line in Figure 3. The pressure in the SVC averaged 2218 N/m^2 or 16.6 mmHg (at peak systole) and 1344 N/m^2 or 10.1 mmHg (at end diastole). It was 1886 N/m^2 or 14.1 mmHg (averaged over the cardiac cycle). Incoming flow from the mBTS increased local WSS to 288 Pa (at peak systole), on the inferior luminal surface of the PAs. The WSS (averaged over the luminal area, and the cardiac cycle) for the central RPA and LPA was 30.8 Pa and 33.1 Pa, respectively, and for the central (RPA plus LPA) was 32.4 Pa. The ΔW (averaged over the cardiac cycle) in the central (RPA plus LPA) totaled 0.14 W. The overall PE for the system was 31 %.

Part III: BGS'S Supplemented with a 4 mm mBTS Connected Directly to the SVC:

In both of these cases, the 4 mm mBTS was envisioned as connected to the SVC. First, it was attached to the medial wall of the SVC at an angle of ~ 45°. The pressure in the SVC averaged 2273 N/m^2 or 17.0 mmHg (at peak systole) and 1348 N/m^2 or 10.1 mmHg (at end diastole). It was 1890 N/m^2 or 14.2 mmHg (averaged over the cardiac cycle). Figure 9a shows the magnitude of the flow velocity, as projected onto the longitudinal (mid-axial) plane of the cavopulmonary pathway, and Fig (9b) the magnitude of the WSS, (both at peak systole). The high velocity (3-4 m/s) mBTS's jet (Figure 9a- red region) diagonally crossed the SVC to strike the lateral luminal wall, where it increased WSS to ~ 80 Pa (Figure 9b insert-green/yellow region). Note WSS is low (dark blue region) throughout most of the PAs. The WSS (averaged over the luminal area, and the cardiac cycle) for the central RPA

and LPA was 18.4 Pa and 9.8 Pa, respectively, and for the central (RPA plus LPA) was 13.6 Pa, which is significantly lower than when the mBTS was connected directly to the PAs, ~ 30 Pa. The ΔW (averaged over the cardiac cycle) in the central (RPA plus LPA) totaled 0.02 W, again considerably lower. The overall PE for the system was 35 %.

The 4 mm mBTS was then attached at the entrance to the SVC, between the R-INV and L-INV. The pressure in the SVC averaged 1990 N/m^2 or 14.9 mmHg (at peak systole) and 1300 N/m^2 or 9.7 mmHg (at end diastole). It was 1710 N/m^2 or 12.8 mmHg (averaged over the cardiac cycle). Figure 9c shows the magnitude of the flow velocity, as projected onto the longitudinal (mid-axial) plane of the cavopulmonary pathway, and (Figure 9d) the magnitude of the WSS, (both at peak systole). The high velocity (3-4 m/s) mBTS's jet (Figure 9c-red region) flowed along the entire axis of the SVC to strike the inferior luminal wall of the RPA, where it created an annular area of high WSS ~ 235 Pa (Figure 9d insert- annular red region surrounding a stagnation point in blue). The WSS (averaged over the luminal area, and the cardiac cycle) for the central RPA and LPA was 48.7 Pa and 12.5 Pa, respectively, and for the central (RPA plus LPA) was 29.5 Pa. The ΔW (averaged over the cardiac cycle) in the central (RPA plus LPA) totaled 0.08 W. The overall PE for the system was 33 %.

Discussion

The BGS'S (SVC to RPA) is commonly employed as temporary surgical palliation for patients with functional single ventricle. Insomuch as the BGS'S alone may not provide sufficient blood flow to the lungs, it has become customary, in some patients, to include an additional source of pulmonary blood flow, often by incorporating a mBTS usually to the LPA. In this study, we focused on the mBTS's effect on the blood flow-vessel wall shearing interaction, as reflected in WSS. Knowledge of the WSS within the cavopulmonary pathway is important, as it is an accepted metric for identifying sites related to a higher risk of thrombus formation and/or fibrointimal hyperplasia.

Incorporating clinical information into numerical calculations is crucial for obtaining results that accurately reflect patients' situation. Thus, an important aspect of this investigation was to utilize patient-related data to describe the inlet and outlet boundary conditions [11]. In earlier fluid dynamics studies of a BGS'S alone [9,10], the velocity profile at the inlet to the SVC was assumed to be parabolic, which would be indicative of fully developed flow. An alternative approach has been to use a rectangular velocity profile at the inlet, but considerably lengthen the SVC to obtain a more- realistic flow pattern as flow enters the region of interest. These choices are unsatisfactory for two reasons: 1) the length required to achieve a parabolic velocity profile at the inlet to the SVC is significantly greater than the anatomic distance available, *in vivo* and 2) more importantly, the actual velocity profile at the inlet to the SVC would be expected to be significantly influenced by blood flow returning from the major systemic veins leading into the SVC. To overcome this difficulty, we extended our computational domain to include the R- and L- IJVs, R- and L- SCVs and R- and L- INVs.

For a BGS'S alone, Figure 10a shows the velocity profile at the inlet to the SVC, arising as a consequence of flow mixing from the extended systemic venous system. Figure 10b shows the resultant velocity distribution that emerges, as projected onto the cross-sectional plane at the axis of the SVC. In contrast, Figure 10c shows an assumed parabolic velocity profile at the inlet to the SVC. Figure 10d shows the corresponding velocity distribution, again as projected onto the cross-sectional plane at the axis of the SVC. In both cases, net flow rate

Entering the SVC was 1L/min. The difference between the two velocity distributions is dramatic. By including the extended venous system, the velocity profile at the inlet to the SVC, Figure 10a, had an asymmetric shape, because of the difference in orientation of the INVs. The prominent peak in the velocity profile reflects the more rightward- streaming flow from the INVs. The resultant velocity distribution, Figure 10b, is relatively uniform (note unidirectional small black arrows in the green region), indicating decelerating flow (yellow to green to blue regions) into the RPA. In contrast, the assumed parabolic velocity profile at the inlet to the SVC, Figure 10c, has an axially symmetric shape. The corresponding velocity distribution, Figure 10d, contains a broad central jet (red region), which gives rise to counter-rotating flow-velocity fields (large curved black arrows) in the cross- sectional plane of the RPA, an unlikely pattern for the systemic venous pathway.

Our CFD analysis has shown that a mBTS's pulsatile high-velocity jet interacting with a BGS'S's passive low-velocity flow can create a power- depleting hemodynamic environment within the central PAs (Figure 7a,b). The jet from the mBTS enters the LPA and strikes the inferior luminal wall, where it drives flow along the anterior and posterior side walls of the vessel (Figure 7a, large curved black arrows)*,**. These secondary currents in the cross-sectional plane of the LPA evolve into counter-rotating vortices, which augment WSS by increasing local flow velocity gradients. Due to viscosity, these vortices dissipate energy in their circular motion along the PAs***. Downstream from the mBTS, the low-velocity flow emerging from the BGS'S (blue/green region) interacts with the approaching flow from the LPA to form complex interconnecting vortices, which penetrates into the SVC.

**In actuality, the incoming jet from the mBTS exhibits a pendulum-like motion in the cross-sectional plane of the LPA during the cardiac cycle, due to cyclic changes in elastic shear stress sustained by the jet, see supplementary Video.*

***The evolution of these counter rotating vortices is similar to what occurs when flow traverses a curve or bend in a vessel. In our case, the mBTS provides the intrusive jet required to initiate the counter rotating vortices in the cross-sectional plane of the LPA; whereas, at a prominent bend in a vessel, centrifugal effects create the outward jet needed to establish vortices.*

****Counter-rotating vortices tend initially not to merge. This follows since the fluid currents between the two axes of rotation move in the same direction and thus have no simple way to dissipate energy yet maintain angular momentum. Hence, the counter-rotating vortices initially tend to remain apart.*

The PA luminal surface is a dynamic, metabolically-active interface. It is largely regulated by the flow of blood, which

influences endothelial cell function through molecular responses to the imposed WSS. Abnormally high shearing forces can trigger endothelial cells to assume a pro-thrombotic character and/or to undergo excessive proliferation, which can lead to clot formation and/or fibro intimal hyperplasia. Both of these processes eventually can compromise luminal patency [14].

Under normal hemodynamic conditions, pulsatile WSS is a potent stimulus for: 1) PA endothelial production of the vasodilator nitric oxide, 2) vascular recruitment and 3) lung growth; all of which can influence pulmonary vascular resistance. For the BGS'S alone, we found WSS, averaged over the luminal surface of the central PAs, to be ~ 0.9 Pa, which is comparable to values reported by Troianowski et al., ~ 1 Pa, in single-ventricle patients with a BGS'S alone [11]. These values are low compared to the WSSs determined by Tang et al. [27] in normal individuals, 2-3 Pa [28]. This result seems plausible, insomuch as pulmonary blood flow in Glenn patients is passive and of low velocity.

A lower than normal WSS in the PAs of Glenn patients, however, can have unfavorable effects on vascular function. Chronic privation of pulsatile pulmonary blood flow has been shown to reduce the PA endothelium's production of nitric oxide by decreasing expression of constitutive nitric oxide synthase [29]. In patients with a BGS'S alone, Kurotobi et al. [30] found PA endothelial – dependent relaxation to acetylcholine, which is contingent upon endogenous nitric oxide release, to be significantly reduced; whereas, the endothelial non-dependent relaxation to nitroglycerin was well preserved. Such endothelial dysfunction could impair basal PA tone and effectively elevate pulmonary vascular resistance, a critical factor in Glenn patients. It remains unclear whether and how the Pas ultimately adjusts to Fontan circulation; however, abnormal WSS, either high or low, and present even at the BGS'S stage, may be an important factor regulating that process.

For the modeled BGS'S supplemented with a 4 mm mBTS, we found WSS, (averaged over the luminal area, and the cardiac cycle) for the central RPA and LPA to be 6.2 Pa and 53.7 Pa, respectively, compared to ~ 0.9 Pa for a BGS'S alone. Juxtaposed to the insertion of the mBTS into the LPA, local WSS dramatically increased to 280 Pa, at peak systole, (Figure 7). Such an abnormally high WSS can induce conformational changes in endothelial cells, which upregulate their expression of coagulatory molecules, such as von Willebrand factor, Factor VIII and tissue factor [31]. Moreover, harsh shearing forces can lead to an unfolding of von Willebrand factor, which facilitates its release of pro-thrombotic Factor VIII [32] and enhances its binding to the platelet membrane glycoprotein GP(Ib) complex, the irreversible step in platelet aggregation [33].

Endothelial cells are sensitive not only to the magnitude of the WSS, but also the spatial WSS gradient (WSSG), and the sign of the gradient. By spatial WSSG, we mean the change in the magnitude of the WSS, along the flow direction, with respect to stream-wise distance. Dolan et al. [13,14,31], using a flow chamber, compared effects on vascular endothelial cell layers exposed to high WSS in the absence of a WSSG (steady flow) to those obtained when the imposed WSS was associated with a positive WSSG (accelerating flow) or a negative WSSG (decelerating flow). Their results demonstrate that an associated positive WSSG can significantly worsen and a negative WSSG markedly lessen high WSS's deleterious effects on endothelial cell structure and function. Current findings [14] suggest accelerating flow imposes a stretching of the endothelial cell surface; whereas, decelerating flow leads to a compression of the surface. These contrasting responses augment or diminish, respectively, the flow field's shearing effects on endothelial cells. It appears a stretching of the cell surface has a greater propensity to disrupt cell-cell junctions and intercellular signaling than does a compressing of the surface [13,14].

Our calculations indicate that flow from a left mBTS creates high WSS on the luminal surface of the LPA (Figure 7). Such a localized region of abnormal WSS would most likely develop narrowing and may require stenting and/or surgical augmentation. However, the high WSS was found to rapidly diminish as flow progressed from the LPA (57.3 Pa) to the RPA (6.2 Pa), implying a large negative WSSG (~ - 4,300 Pa/m) indicative of decelerating flow. Thus, given the recent empirical findings of Dolan et al [13,14], it is likely that functional integrity of the PAs would be relatively preserved when a BGS'S is supplemented with a mBTS [13,14].

For the BGS'S alone, the power dissipated in the central Pas totaled ~ 0.20 mW, which reflects the low power delivered by the BGS'S and the high PE (96%). This power loss is comparable to that reported by Pekkan et al. [34], ~ 0.17 mW, for patient-specific computational Glenn models. In contrast, for the 4 mm mBTS alone, the power dissipated in the central Pas (averaged over the cardiac cycle) was ~ 0.14 W, which reflects the high power delivered by the mBTS and the low PE (31%) [36,36]. Lastly, for the BGS'S supplemented with a 4 mm mBTS, the power dissipated in the central Pas also totaled ~ 0.14 W. Thus, WSS associated with flow from the mBTS becomes the primary source of viscous energy dissipation in the PAs. Nevertheless, the remaining power available to stimulate growth of distal PA vessels is ~ 4 times greater for the BGS'S with a mBTS than for a BGS'S alone[37,38].

Although the mBTS delivers pulsatile flow to the lungs, the shunt's high velocity jet gives rise to cyclic vortices in the PAs that markedly increase local WSS. One way to avoid this situation would be to connect the mBTS directly to the SVC. Although this approach may seem unorthodox, several investigators have recently suggested employing a small shunt from the innominate artery to the SVC, as a means of harvesting the shunt's high kinetic energy to entrain BGS'S flow [39,40]. We first considered the mBTS to be anastomosed to the medial aspect of the SVC at an angle of ~ 45°. By repositioning the mBTS in this manner, the high WSS is created on the lateral luminal wall of the SVC (Figure 9b). It is plausible, this relocation of the high WSS may impair less SVC's primary role as a conduit for systemic venous flow, than it would have PA's function as a vasoactive vessel. We then took the mBTS to be connected to the SVC, between the insertions of the INVs. The high velocity jet from the mBTS, rather than dispersing in the SVC, remained intact as it flowed along the entire length of the cava to create high WSS on the inferior luminal wall of the RPA (Figure 9d). This arrangement simply shifts the high WSS burden from the LPA to the RPA.

Table 1 Major systemic veins providing blood flow to the SVC, labels are defined in the text.

	Diameter (mm)	Length (mm)	Flow Rate (L/min)
R-SCV	4.9	20	0.19
R-IJV	6.9	20	0.28
L-SCV	4.9	20	0.22
L-IJV	6.9	20	0.31
R-INV	9.8	10	0.47
L-INV	9.8	32	0.53
SVC	12.5	39	1.0

Table 2 Planar model of the BGS with a 4 mm left mBTS in part (I). Figure 1 Summary of clinically-important hemodynamic parameters. *Averaged over the luminal area of the vessel (s). The central PA first-order branch representative pressure (averaged over the cardiac cycle) is 12 mmHg. The pressures, expressed in N/m2, are provided in the Results Section of the text. Q=Flow rate. WSS=Wall shear stress. The marked disparity in the magnitude of the WSS between the RPA (6.2 Pa) and LPA (53.7) cannot be explained by the disparity in their flow rates, created by the addition of the mBTS.

	BGS Alone	BGS with 4 mm Left mBTS (Figure 1)		
		Peak Systole	End Diastole	Averaged Over the Cardiac Cycle
Average Pressure in the SVC (mmHg)	12.3	16.4	10.2	14.3
Average Pressure in the central RPA (mmHg)	12.2	15.7	9.8	13.8
Average Pressure in the central LPA (mmHg)	12.2	15.0	9.2	12.9
Average Pressure in the mBTS (mmHg)	-	29.6	16.4	22.4
Q_{SVC} (L/min)	1	1	1	1
Q_{mBTS} (L/min)	-	2.24	1.45	1.82
Q_{RPA} (L/min)	0.55	1.73	1.37	1.55
Q_{LPA} (L/min)	0.45	1.51	1.08	1.27
WSS_{SVC} (Pa)*	0.7	0.8	0.8	0.8
WSS_{RPA} (Pa)*	1.2	9.7	4.6	6.2
WSS_{LPA} (Pa)*	0.7	78.1	36.6	53.7
$WSS_{RPA+LPA}$ (Pa)*	0.9	44.5	20.9	30.4
WSS_{mBTS} (Pa)*	-	37.3	21.0	28.4

Table 3 a) Pressure averaged within the SVC, and then averaged over the cardiac cycle. b) Pressure averaged within the central (RPA + LPA), and then averaged over the cardiac cycle. c) Wall shear stress (WSS) averaged throughout the luminal area of the central (RPA + LPA), and then averaged over the cardiac cycle. d) Power loss totaled within the central (RPA + LPA), and then averaged over the cardiac cycle. (Representative pressure at the central RPA and LPA first- order branch outlets are 12 mmHg, when averaged over the cardiac cycle (Figure 2).

	(a) Pressure in SVC (mmHg)	(b) Pressure in (RPA+LPA) (mmHg)	(c) WSS in the (RPA+LPA) (Pa)	(d) ΔW in the (RPA+LPA)(W)
BGS alone	12.3	12.2	0.9	0.2×10^{-3}
BGS with a 4 mm left mBTS (Figure 1)	14.3	13.4	30.4	0.14
BGS with a repositioned 4 mm left mBTS to the origin of the RPA and LPA	14.0	13.0	31.5	0.14
BGS with a 5 mm left mBTS (Figure 1)	15.5	14.0	39.4	0.21
BGS with a 4 mm left mBTS, and an angulated LPA (Figure 3)	13.9	12.9	29.3	0.11
BGS with a repositioned 4 mm left mBTS to the origin of the RPA and LPA and an angulated LPA	14.1	13.1	32.4	0.14
BGS with a 4 mm mBTS connected directly to the medial side of the SVC at ~45^0	14.2	13.2	13.6	0.02
BGS with a 4 mm mBTS connected, between the INVs, directly to the SVC	12.8	12.9	29.5	0.08

Table 3 summarizes important hemodynamic parameters, as averaged over the cardiac cycle, for the various cases studied. SVC pressure modestly increased, to ~ 14 mmHg, with the addition of a supplementary 4 mm mBTS. However, in all cases except one, WSS in the central PAs was high at ~ 30 Pa, vs ~ 0.9 Pa for a BGS'S alone and 2-3 Pa for normal hearts. For the mBTS inserted

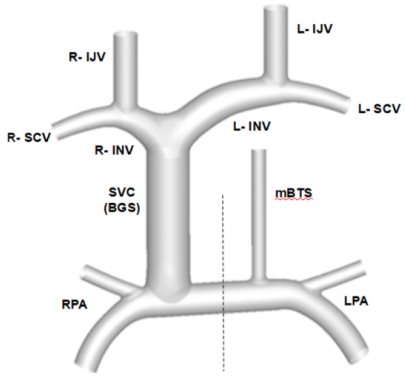

Figure 1 Schematic reproduction of a BGS supplemented with a 4 mm left mBTS. The diameters and lengths of the vessels are defined in the text, and are summarized in Table 1. The dashed vertical line denotes the origin of the RPA and LPA. Labels are described in the text.

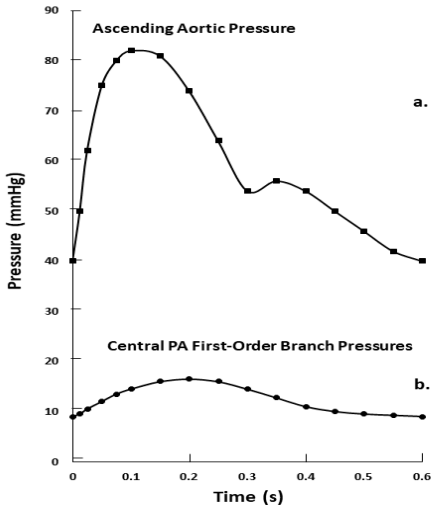

Figure 2 Pressures, in mmHg, vs. time, in seconds, during one cardiac cycle, used for the boundary conditions: a) the representative aortic pressure tracing (which averaged 59.3 mmHg) taken at the inlet to the mBTS (upper curve) and b) the representative PA pressure tracing (which averaged 12 mmHg) used at the outlets of each of the central RPA and LPA first-order branches (lower curve). The cycle length is 0.6 s, which corresponds to a heart rate of 100 bpm. PA = pulmonary artery.

at the origin of the PAs, because of the spatial symmetry of the arrangement, WSS was comparable in magnitude and distribution for the RPA and LPA, i.e. 31.6 Pa and 31.5 Pa, respectively (Figure 11). Interestingly, when the mBTS was connected directly to the SVC at ~ 45°, SVC pressure also increased to ~ 14 mmHg, but WSS in the PAs remained low at 13.6 Pa and ΔW was only 0.02 W. Nevertheless, in all cases, WSS uniformly decreased as flow progressed along the PAs. Such a declining shear stress has been shown, in vitro, to lessen endothelial cell dysfunction [13,14].

The main benefits of a BGS'S is it improves effective pulmonary blood flow and reduces the work required of the heart by

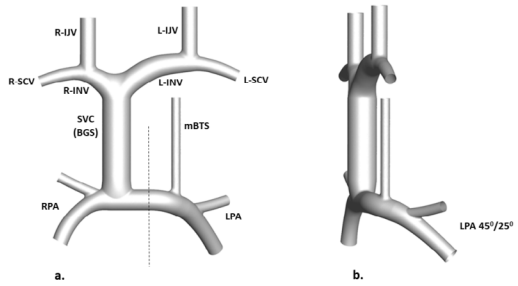

Figure 3 Schematic reproduction of a BGS supplemented with a 4 mm left mBTS with the LPA angulated. Based on angiography, the axis of the LPA was rotated posteriorly (~45°) and inferiorly (~25°), with respect to the axis of the RPA. The Fig in the lateral view has been oriented to better display the spatial position of the LPA. The diameters and lengths of the vessels are the same as those in Fig 1. The dashed vertical line denotes the origin of the RPA and LPA. Labels are described in the text.

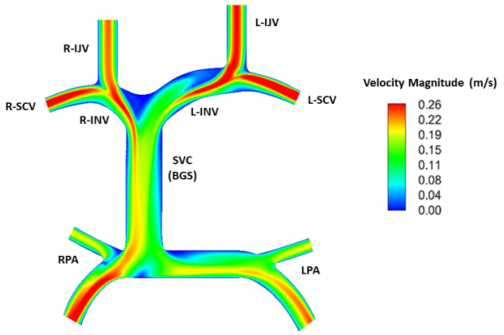

Figure 4 Magnitude of the flow velocity, in m/s, as projected onto the longitudinal (mid-axial) plane of the cavopulmonary pathway, for the BGS alone. Note streaming of flow (red/yellow regions) towards the RPA, due in part to the relative orientation of the INVs. Labels are described in the text.

decreasing preload on the single ventricle. It also helps preserve ventricular diastolic function, as any impairment of which could critically affect Fontan performance. Moreover, the BGS'S can provide time for remodeling of the ventricular myocardium prior to completion of the Fontan procedure. The primary disadvantage of a BGS'S is that pulmonary blood flow is non- pulsatile and of low velocity, thereby lacking sufficient vis a tergo to promote optimal growth of the PAs. The outcome following the Fontan procedure largely depends on patient selection. However, among the criteria for successful Fontan completion, adequate PA size is paramount.

Small PAs are common in patients with single ventricle, particularly the LPA, and frequently require surgical augmentation. However, such repairs tend to be unrewarding, in the low pressure, low flow cavopulmonary pathway. Most studies [35], but not all [36], find underdeveloped PAs to be hemodynamically disadvantageous after Fontan completion. Kansy et al. [37], based on angiography, found the mean Nakata index pre- BGS'S to be 351.9 mm^2/m^2; whereas, a few years following placement of the BGS'S, the index

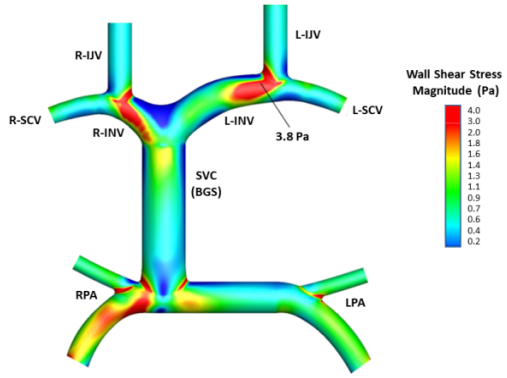

Figure 5 Contour plot of the magnitude of the WSS, in Pa, throughout the cavopulmonary pathway, for the BGS alone. Note increase in WSS to ~ 2 Pa (red regions), where flow undergoes an abrupt change in direction. Labels are described in the text.

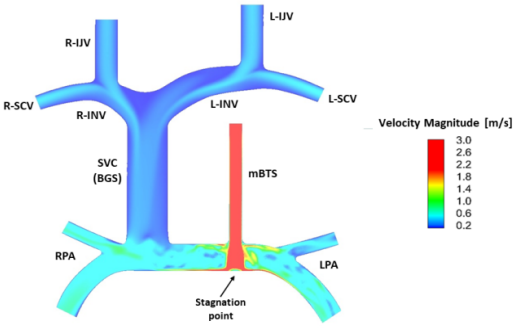

Figure 6 Magnitude of the flow velocity, in m/s, as projected onto the longitudinal (mid-axial) plane of the cavopulmonary pathway, for the BGS supplemented with a 4 mm left mBTS, shown in Fig (1), at peak systole. Note increase in velocity to ~ 0.6 m/s in the central PAs (light blue regions), due to flow from the mBTS. The high velocity jet (3-4 m/s) in the mBTS (red region) passes across the LPA, strikes its inferior wall and subsequently gives rise to counter- rotating vortices (not seen in this view, but see text). Labels are described in the text.

decreased to 226.4 mm²/m². Some of this reduction in index may be a reflection of the decrease in pulmonary blood flow. Recently, however, Seaman et al. [38] successfully treated 12 single ventricle patients with a BGS'S alone and diffuse hypoplasia of the LPA. The LPA was ligated at its origin and a mBTS was connected at that site. The arterial shunting increased the caliber of the LPA from 4.1 mm (median for the BGS'S alone) to 6.7 mm (median post-mBTS), and without further change in size following the Fontan [40].

In our study, we chose reported flow rates for systemic veins leading to the SVC, and representative pressures for the inlet to the mBTS and at the outlets of the PA first-order branches, to inform boundary conditions for the CFD calculations. This approach resulted in BGS'S and mBTS flow rates (1-2 L/min), which are similar to those determined using cardiac catheterization data in conjunction with Doppler flow- velocity analyses [41].

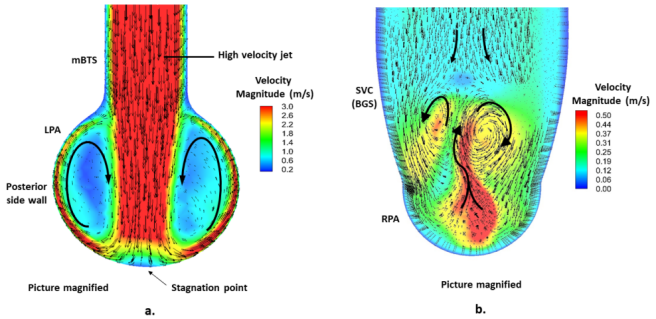

Figure 7 a) Magnitude of the flow velocity, in m/s, as projected onto the cross-sectional plane, at the axis on the left mBTS, for the BGS supplemented with a 4 mm left mBTS, shown in Fig (1), at peak systole. Viewing is from anatomical R to L. The emerging counter-rotating vortices are shown. The small black arrows indicate direction of flow. The larger curved black arrows signify flow's direction of rotation. b) Magnitude of the flow velocity, in m/s, as projected onto the cross-sectional plane, at the axis of the SVC, at peak systole. Again, viewing is from anatomical R to L. The small black arrows indicate direction of flow. Here, the larger curved black arrows depict the interwoven flow patterns that emerge, as the SVC stream mixes with advancing flow from the LPA. Labels are described in the text.

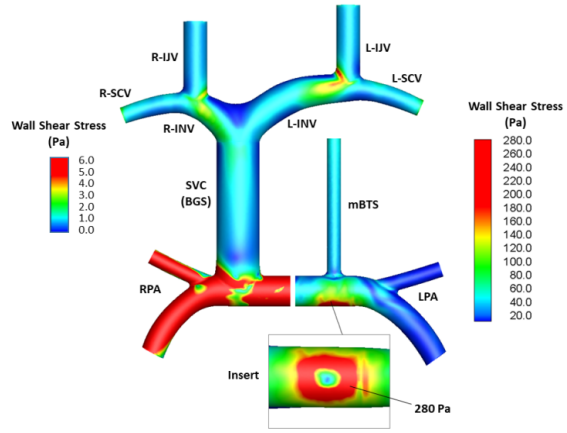

Figure 8 Contour plot of the magnitude of the WSS, in Pa, throughout the cavopulmonary pathway, for the BGS supplemented with a 4 mm left mBTS, shown in Fig (1), at peak systole. The figure has been divided between the central RPA and LPA to better illustrate the range in magnitude of the WSS. Note the difference in WSS scale for the BGS- RPA part (on the left of the Fig) and the mBTS- LPA part (on the right of the Fig). The insert (lower part of the Fig) depicts the annular area (red region) of markedly elevated WSS (280 Pa) surrounding a stagnation point (tiny dark blue area), juxtaposed to the insertion of the mBTS into the LPA. Labels are described in the text.

Since systemic venous flow entering the SVC was fixed, intrusion of flow from the mBTS into the SVC was primarily reflected by increases in SVC pressure, (Table 3). An alternative approach could have been to specify pressures in the systemic veins, although less-well defined, and alter flow rate in the mBTS. Intrusion of

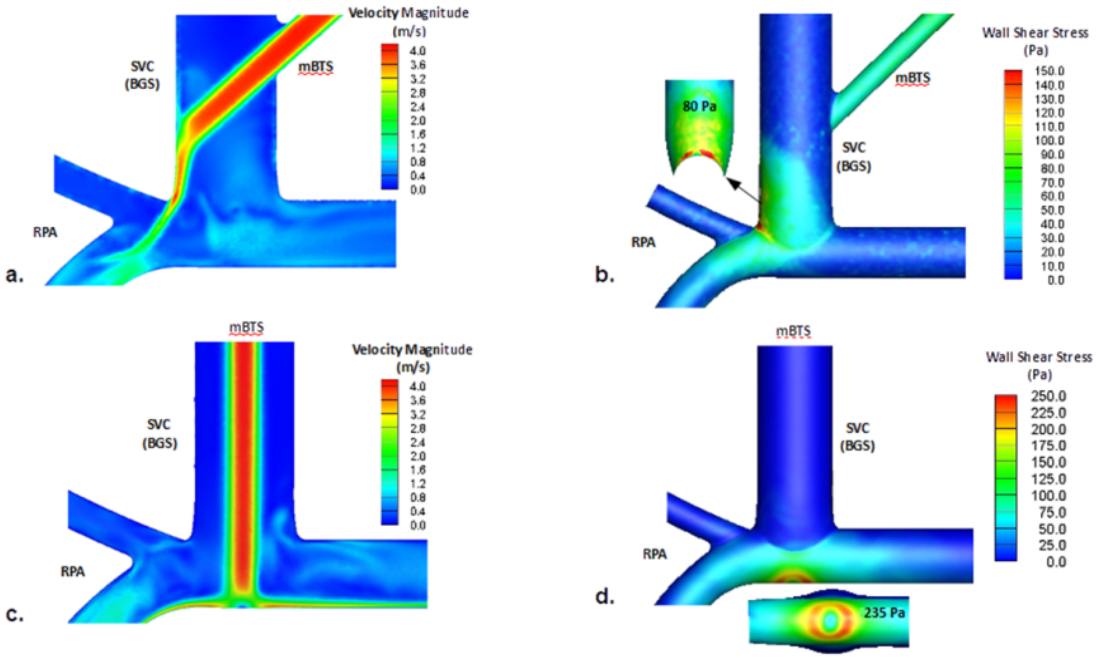

Figure 9 a) Magnitude of the flow velocity, in m/s, as projected onto the longitudinal (mid-axial) plane of the cavopulmonary pathway, with a 4 mm mBTS connected directly to the medial wall of the SVC at an angle of ~ 45%, at peak systole. b) Contour plot of the corresponding WSS, in Pa. c) Magnitude of the flow velocity, in m/s, as projected onto the longitudinal (mid-axial) plane of the cavopulmonary pathway, for a 4 mm mBTS connected directly to the SVC between the INVs, at peak systole. d) Contour plot of the corresponding WSS, in Pa. See text.

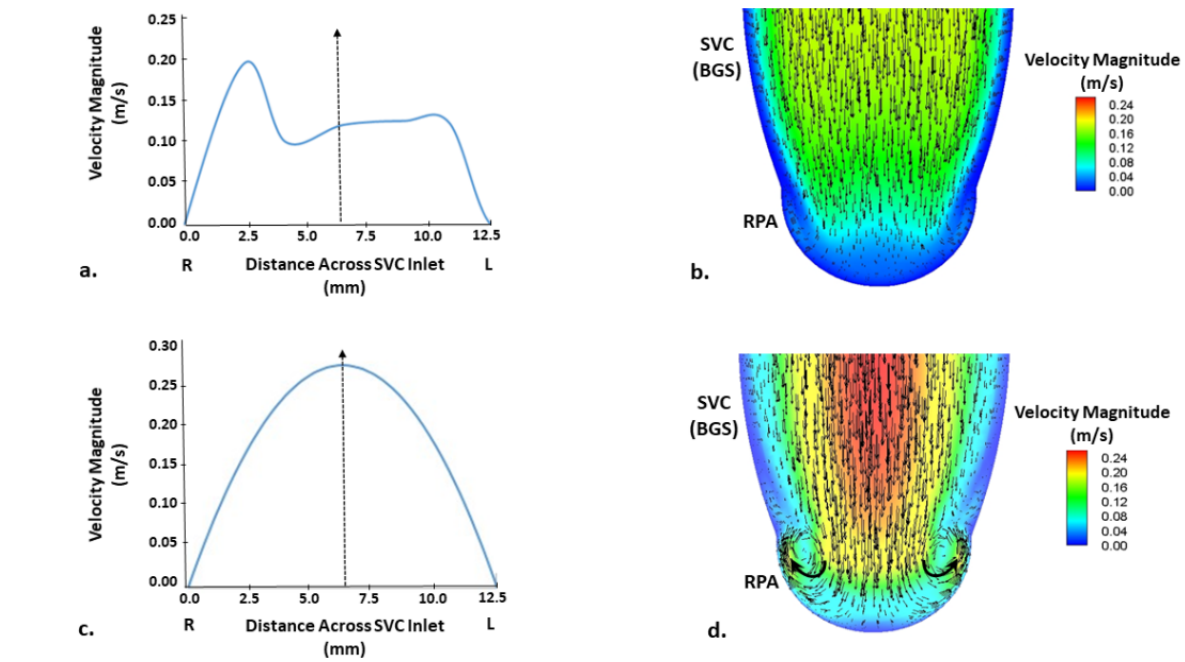

Figure 10 a) Flow-velocity profile, in m/s, at the inlet to the SVC, arising as a consequence of flow mixing from the extended venous system and b) the resulting velocity distribution, as projected onto the cross-sectional plane, at the axis of the SVC; c) Assumed parabolic flow-velocity profile, in m/s, at the inlet to the SVC and d) the resulting velocity distribution, as projected onto the cross-sectional plane, at the axis of the SVC. A broad central jet (red region) gives rise to counter-rotating vortices at the junction of the SVC and RPA. The small black arrows indicate direction of flow. The larger curved black arrows signify the direction of rotation of flow. R = Anatomical right side and L = Left side of the SVC. For visual purposes, the SVC has been foreshortened.

flow from mBTS flow into the SVC would then become realized through decreases in SVC flow. Comparing local hemodynamics using these alternative boundary prescriptions deserves future evaluation.

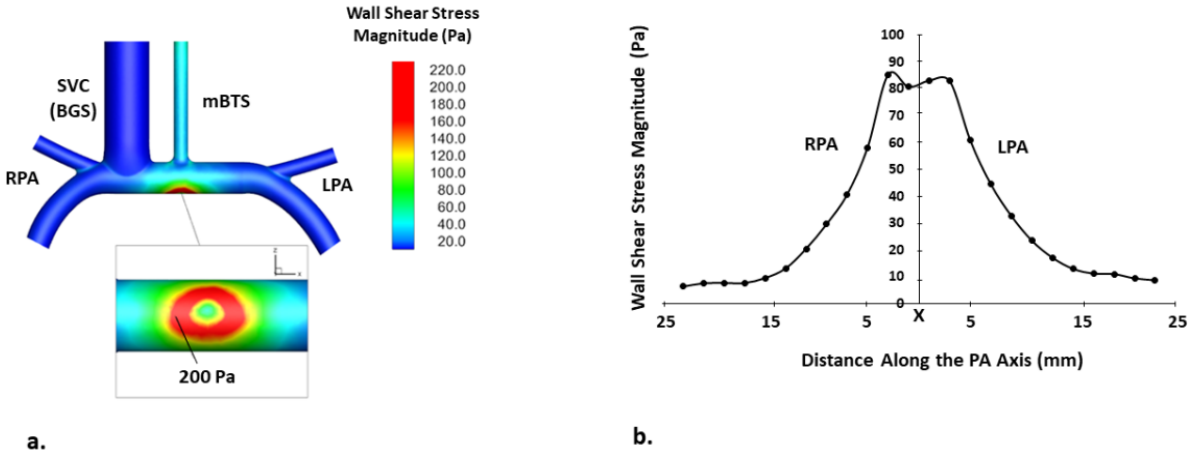

Figure 11 a) Contour plot of the magnitude of the WSS, in Pa, averaged over the cardiac cycle, throughout the cavopulmonary pathway, for the BGS supplemented with a 4 mm mBTS, which is now located at the origin of the RPA and LPA. In the figure, the SVC and the mBTS have been foreshortened to better display the WSS distribution in the PAs, and on the inferior luminal wall (insert), juxtaposed to the insertion of the mBTS, see also insert in Fig 8. b) Magnitude of the WSS, in Pa, vs. distance, in mm, along the axis of the PAs, from the origin (X) of the central RPA (and LPA) to their first-order branches. To calculate the WSS values shown, we divided each of the central PAs into 12 rings, each 2 mm in width, at consecutive location along their axes (black dots). The WSS distribution on each ring was then averaged over the luminal wall, and the cardiac cycle.

Flow rates or pressures were suitably included at sites considerably proximal to the inlets of the simulated cavopulmonary pathway. However, specifying pressure alone at the outlets may not adequately account for conditions beyond the PA first-order branches. Under these circumstances, rather than assigning representative pressure at the outlet boundaries, the 3D-solver for the N-S equations could be linked to additional computational components that are encoded to represent characteristic features (resistance, capacitance and impedance) of the distal circulation[42]. Thus, the 3D-solver's output data can provide input for the accessory components, and vise-versa. Such closed loop systems are worthy of consideration; however, they require extensive adjustment of geometric and hemodynamic parameters, which goes beyond the scope of the present investigation.

Summary

In this study, we employed CFD, in conjunction with computer reproductions of cavopulmonary pathways, to characterize pulsatile blood flow in a BGS'S supplemented with a mBTS. Our focus was on hemodynamic WSS and power loss, as these are important determinates of PA growth and lung perfusion. We obtained calculated values of these quantities that are in good agreement with those estimated, *in vivo,* in patients with a BGS'S alone. Inclusion of a mBTS was found to moderately increase pressure and disrupt flow in the SVC. However, the pulsatile high-velocity jet from the mBTS mixing with steady low-velocity flow from the BGS'S gave rise to counter- rotating, power-depleting vortices in the central PAs, which can elevate WSS to levels conducive to endothelial cell dysfunction, thrombus formation and excessive power loss. Although these findings are concerning, the WSS distributions in the central PAs were found to decrease as a consequence of the decelerating flow, which has been shown to ameliorate shearing's deleterious effects on the endothelium. Interestingly, connecting the mBTS directly to the SVC resulted in lower WSS and less energy loss in the PAs. We believe the traditional practice of supplementing a BGS'S with a mBTS, for the limited time required, can be beneficial for promoting PA growth, by restoring pulsatile blood flow and creating cyclic pressure stretch on the luminal vessel wall. Our results do emphasize the need for close surveillance of these Fontan patients. Certainly, additional clinical and computational studies will be required to assess flow's effect on PA function in patients who previously underwent a BGS'S supplemented with a mBTS. Such information is becoming of increasing importance, as the population of surviving single ventricle patient's increases.

Acknowledgement

Supported in part by a grant from the Board of Regents Support Fund, State of Louisiana, (LSEQF-RD-A-18).

References

1 Haller JA, Adkins JC, Worthington M, Ravenhorst J (1996) Experimental studies on permanent bypass of the right heart. Surgery 59: 1128-1132.

2 Mainwaring RD, Lamberti JJ, Uzark K (1994) The bidirectional Glenn: palliation of the univentricular heart. Adv Card Surg 5: 115-140.

3 Lamberti JJ, Spicer RL, Waldman JD, Grehi TM, Thompson D, et al. (1990) The bidirectional cavopulmonary shunt. J Thorac Cardiovasc Surg 100: 22-30.

4 Mendelsohn AM, Bove EL, Lupinetti FM, Crowley DC, Lloyd TR, et al. (1994) Central pulmonary artery growth patterns after bidirectional Glenn procedure. J Thorac Cardiovasc Surg 107: 1284-1290.

5 Yoshida M, Yamaguchi M, Yoshimura N, Murakami H, Matsuhisa H, et al. (2005) Appropriate additional pulmonary blood flow at the bidirectional Glenn procedure is useful for completion of the total cavopulmonary connection. Ann Thorac Surg 80: 976-981.

6 McElhinney DB, Marianeschi SM, Reddy VW (1998) Additional pulmonary blood flow with the bidirectional Glenn anastomosis: does it make a difference? Ann Thorac Surg 66: 668-672.

7 Mainwaring RD, Lamberti JJ, Uzark K, Spicer RL (1999) Bidirectional Glenn. Is accessory pulmonary blood flow good or bad? Circulation 9: 294-297.

8 Webber SA, Horvath P, LeBlanc JG, Slavik Z, Lamb RK, et al. (1995) Influence of competitive pulmonary blood flow on bidirectional superior cavopulmonary shunt. Circulation 92: 279-286.

9 Migliavacca F, de Leval MR, Dubini G, Pietrabissa R (1996) A computational pulsatile model of the bidirectional cavopulmonary anastomosis: the influence of pulmonary forward flow. J Biomech Eng 118: 520-528.

10 Sun Q, Wan D, Liu J, Liu Y, Zhu M, et al. (2008) Numerical simulation of a bidirectional cavopulmonary anastomosis connection with antegrade pulmonary blood flow. IFMBE Proceedings 19: 139-142.

11 Troianowski G, Taylor CA, Feinstein LA, Vignon-Clementel E (2011) Three-dimensional simulations in Glenn patients: clinically based boundary conditions, hemodynamic results and sensitivity to input data. J Biomech Eng 133: 1-16.

12 Davies PF (2009) Hemodynamic shear stress and the endothelium in cardiovascular pathphysiology. Nat Clin Pract Cardiovasc Med Jan 6: 16-26.

13 Dolan JM, Meng H, Singh S, Paluch R, Kolega J (2011) High fluid shear stress and spatial shear stress gradients affect endothelial proliferation, survival and alignment. Ann Biomed Eng Jun 39: 1620-1631.

14 Dolan JM, Kolega J, Meng H (2013) High wall shear stress and spatial gradients in vascular pathology: a review. Ann Biomed Eng 41: 1411-1427.

15 Jai L, Wang L, Wei F, Yu H, Dong H, et al. (2015) Effects of wall shear stress in venous hyperplasia of arteriovenous fistulae. Nephrology May 20: 335-342.

16 Moyle KR, Mallinson GD, Occleshaw CJ, Cowan BR, Gentles TL (2006) Wall shear stress is the primary mechanism of energy loss in Fontan connection. Pediatr Cardiol 27: 309-315.

17 Snajeev S, Karpawich PP (2006) Superior vena cava and innominate vein dimensions in growing children. Pediatr Cardiol 27: 414-419.

18 Oh MH, Chung WS, Kim YH, Kim BM, Park S (2014) Ultrasonographic measurement of subclavian vein diameter and regression modeling in pediatric patients from a single Korean facility. Korean J Anesthesiol 67: S96-S97.

19 Sayin MM, Mercan A, Koner O, Celebi S, Sozubir S, et al. (2008) Internal jugular vein diameter in pediatric patients: are J-shaped guidewire diameters bigger that internal jugular vein? An evaluation with ultrasound. Paediatr Anaesth Aug 18: 745-751.

20 Eksioglu AS, Tasci Yildiz Y, Senel S (2014) Normal sizes of internal jugular veins in children/adolescents aged birth to 18 years at rest and during Valsalva maneuver. Eur J Radiol Apr 83: 673-679.

21 Pettersen MD, Du W, Skeens ME, Humes RA (2008) Regression equations for calculation of Z scores of cardiac structures in a large cohort of healthy infants, children and adolescents: an echocardiographic study. J Am Soc Echocardiogr 21: 922-934.

22 Hurst JW (2014) Central venous access. In Marino's The ICU Book (4th Edtn.). Lippincott Williams & Wilkins, Philadelphia, USA: 17-39.

23 Chavhan GB, Parra DA, Mann A, Navarro OM (2008) Normal Doppler spectral waveforms of major pediatric vessels. Radio Graphics 28: 691-706.

24 Ciuti G, Righi D, Forzoni L, Fabbri A, Pignone AM (2013) Differences between internal jugular vein and vertebral vein flow examined in real time with the use of multigate ultrasound color Doppler. AJNR Am J Neuroradiol 34: 2000-2004.

25 Munson BR, Young DF, Okiishi TH (2003) Fundamentals of Fluid Mechanics (4th Edtn) Wiley & Sons, New York, USA: 350-352.

26 Tazyukov FK, Kahlaf HA, Hassan JM. (2011) Non-Newtonian Modelsfor Blood Flow through an Arterial Stenosis. Proceedings of the ASME International Mechanical Engineering Congress & Exposition.

27 Tang BT, Fonte TA, Chan FP, Tsao PS, Feinstein JA, et al. (2011) Three-dimensional hemodynamics in the human pulmonary arteries under resting and exercise conditions. Ann of Biomed Eng 39: 347-358.

28 Robbers-Visser D, Helderman F, Strengers JL, von Osch-Gevers L, Kapusta L, et al. (2008) Pulmonary artery size and function after Fontan operation at a young age. J Magnet Resonance Image 38: 1101-1107.

29 Gu Q, Smith DO, Hoo KA (2013) Shear stress effect on endothelial nitric oxide synthase in cultured human umbilical vein endothelial cells J Biomed Sci Engineer 6: 982-986.

30 Kurotobi S, Sano T, Kogaki S, Matsushita T, Miwatani T, et al. (2001) Bidirectional cavopulmonary shunt with right ventricular outflow patency: the impact of pulsatility on pulmonary endothelial function. J Thorac Cardiovasc Surg 12: 1161-1168.

31 Dolan JM, Meng H, Sim FJ, Kolega J (2013) Differential gene expression by endothelial cells under positive and negative stream-wise gradients of high wall shear stress. Am J Physiol Cell Physiol Oct 305: C854-C866.

32 Bonazza K, Rottensteiner H, Schrenk G, Frank J, Allmaier G, et al. (2015) Hear-dependent interactions of von Willebrand factor and Factor VIII and protease ADAMTS 13 demonstrated at a single molecule level by atomic force microscopy. Anal Chem Oct 87: 10299-10305.

33 Gogia S, Neelamegham S (2015) Role of fluid shear stress in regulating VWF structure, function and related blood disorders. Biorheology 52: 319-335.

34 Pekkan K, Dasi LP, deZelicourt D, Sundareswaran KS, Fogel MA, et al. (2009) Hemodynamic performance of stage-2 univentricular reconstruction: Glenn vs. Hemi-Fontan templates. Ann Biomed Eng Jan 37: 50-63.

35 Senzaki H, Isoda T, Ishizawa A, Hishi T (1994) Reconsideration of criteria for the Fontan operation. Influence of pulmonary artery size on postoperative hemodynamics of the Fontan. Circulation Jan 89: 266-271.

36 Baek JS, Bae EJ, Kim WH, Lee JR, Kim YJ, et al. (2011) Pulmonary artery size and late functional outcome after Fontan operation. Ann Thorac Surg Apr 91: 1240-1246.

37 Kansy A, Brzezinska-Rajszys G, Zubrzycka M, Mirkowicz-Malek M, Maruszewski P, et al. (2013) Pulmonary artery growth in univentricular physiology patients. Kardiol Pol 71: 581-587.

38 Seaman C, d'Udekem Y, Jones B, Brizard C, Cheung M (2016) Physiological augmentation of pulmonary arterial growth in patients

with single ventricle physiology with interim selective systemic to pulmonary arterial shunt. Circulation 134: A18380.

39 Esmaily MM, Hsia TY, Marsden AL (2015) A novel surgical approach for first-stage single-ventricle heart palliation. The Journal of Thoracic and Cardiovascular Surgery 149: 699-705.

40 Gervaso F, Kull S, Pennati G, Migliavacca F, Dubini G, et al. (2004) The effect of the position of an additional systemic-to-pulmonary shunt on the fluid dynamics of a bidirectional cavo-pulmonary anastomosis. Cardiol Young 14: 38-43.

41 Celestin C, Guillot M, Ross-Ascuitto N, Ascuitto R (2015) Computational fluid dynamics characterization of blood flow in central aorta to pulmonary artery connections: importance of shunt angulation as a determinate of shear stress-induced thrombosis. Pediatr Cardiol 36: 600-15.

42 Ascuitto R, Ross-Ascuitto N, Guillot M, Celestin C (2017) Computational fluid dynamics characterization of pulsatile flow in central and Sano shunts connected to the pulmonary arteries: importance of graft angulation on shear stress-induced, platelet-mediated thrombosis. Interact Cardiovasc Thorac Surg 25: 414-421.